pubs.acs.org/Biomac

Article

Evaluating Endosomal Escape of Caspase-3-Containing Nanomaterials Using Split GFP

Francesca Anson, Bin Liu, Pintu Kanjilal, Peidong Wu, Jeanne A. Hardy,* and S. Thayumanavan*

Cite This: https://dx.doi.org/10.1021/acs.biomac.0c01767

Read Online

ABSTRACT: The ability for biologics to access intracellular targets hinges on the translocation of active, unmodified proteins. This is often achieved using nanoscale formulations, which enter cells through endocytosis. This uptake mechanism often limits the therapeutic potential of the biologics, as the propensity of the nanocarrier to escape the endosome becomes the key determinant. To appropriately evaluate and compare competing delivery systems of disparate compositions, it is therefore critical to assess endosomal escape efficiencies. Unfortunately, quantitative tools to assess endosomal escape are lacking, and standard approaches often lead to an erroneous interpretation of cytosolic localization. In this study we use a split-complementation endosomal escape (SEE) assay to evaluate levels of cytosolic caspase-3 following delivery by polymer nanogels and mesoporous silica nanoparticles. In particular, we use SEE as a means to enable the systematic investigation of the effect of polymer composition, polymer architecture (random vs block), hydrophobicity, and surface functionality. Although polymer structure had little influence on endosomal escape, nanogel functionalization with cationic and pH-sensitive peptides significantly enhanced endosomal escape levels and, further, significantly increased the amount of nanogel per endosome. This work serves as a guide for developing an optimal caspase-3 delivery system, as this caspase-3 variant can be easily substituted for a therapeutic caspase-3 cargo in any system that results in cytosolic accumulation and cargo release. In addition, these data provide a framework that can be readily applied to a wide variety of protein cargos to assess the independent contributions of both uptake and endosomal escape of a wide range of protein delivery vehicles.

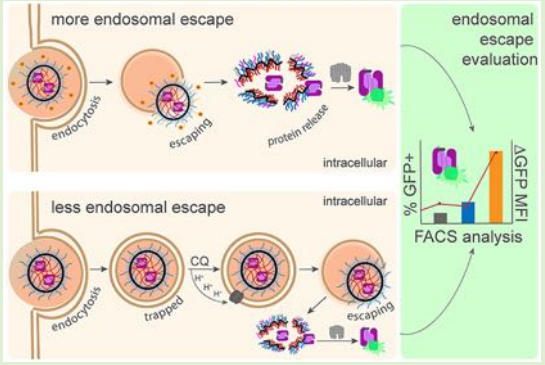

INTRODUCTION

Protein biologics are an important emergent class of pharmaceuticals that have immense therapeutic potential due to their specificity. Nevertheless, using these biologics is challenging because of their degradation in the bloodstream, short half-lives, and the potential for off-target action.[1,2] Thus, biologics often require conjugation within a safe delivery system, utilizing native residues or engineered reactive handles to facilitate intracellular translocation and improved pharmacokinetics.[3,4] Substantial efforts have focused on developing efficient vehicles to deliver biologics via covalent or supramolecular formulation using polymer,[5] dendrimer,[6] lipid, or inorganic materials.[1,7−9] These vehicles provide benefits beyond cellular entry, including cargo protection and cell targeting. Additional requirements include sufficient cytosolic localization of an unmodified biologic while maintaining intrinsic structure and function.[8,10] To better understand the factors that impact delivery efficiencies, it is essential to distinguish cellular uptake followed by cytosolic localization from a simple cellular uptake, which often results in endosomal entrapment.

The overarching hurdle in evaluating intracellular biologic delivery is the dependence on endosomal escape for which robust and quantitative evaluation tools are lacking.[11−13] The field of delivery instead relies heavily on labeled-cargo imaging or end point therapeutic assays to imply intracellular delivery. Microscopy can be used to visualize endosomal entrapment or escape and flow cytometry or total cell lysate analyses can elucidate internalization. Nevertheless, microscopy and flow studies rely on dye-functionalization of delivery vehicles or cargo, affording obstructions from dye-induced hydrophobicity and membrane-association, complicating interpretation.[14−17] For example, our group has observed mitochondrial targeting upon cyanine dye (Cy3) functionalization of anionic polymers.[18] Moreover, the process of cell fixation allows redistribution of endocytotic vesicles, often compromising membrane integrity.[19−21] On the other hand, flow cytometry or total cell lysate analysis solely reveal total internalization,

Received: December 16, 2020
Revised: February 3, 2021

Scheme 1. Split-Complementation Endosomal Escape (SEE) Pathways for NG Delivering Tagged casp-3 (C3-11)[a]

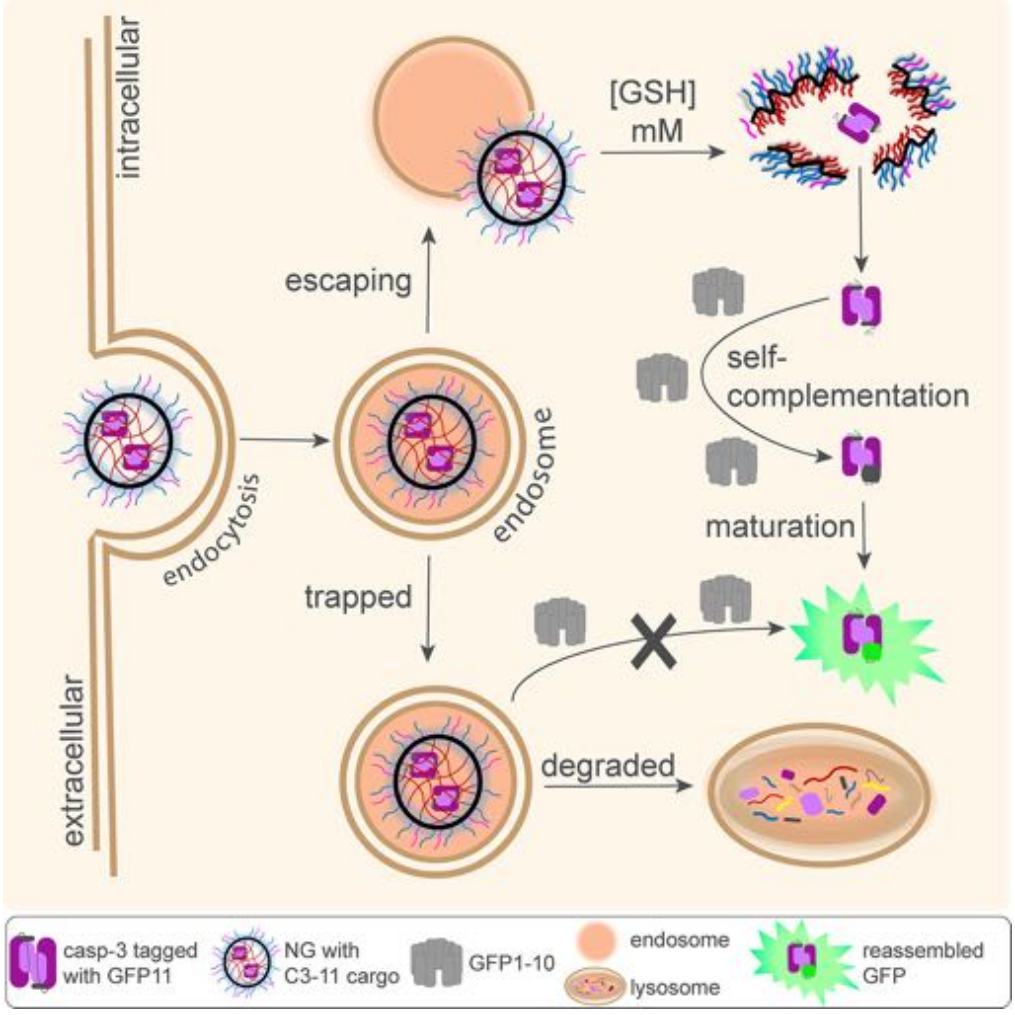

[a]Only once nanogels (NG) escape the endosome into the cytosol will C3-11 be released, by cytosolic glutathione, leading to reassembly with cytosolically expressed GFP1-10 and generation of GFP fluorescence.

regardless of cytosolic or endosomal localization. Therefore, alternative methods, such as the use of split GFP, have recently been investigated to reveal true cytosolic translocation of protein cargos and antibodies.[22−27]

Significant endosomal escape is related to cargo concentration in each endosome as well as the number of endosomes containing the delivered agent.[11,28] Many efforts have focused on enhancing these parameters by incorporating moieties within delivery systems that induce endosomal membrane fusion, membrane destabilization, or osmotic rupture through the proton sponge effect.[11,13,29] Delivery systems must rely on a balance of membrane influence with cytotoxicity as there is typically a correlated relationship. The field of delivery would significantly benefit from routine use of assays that directly evaluate and quantify endosomal escape, despite the challenges and increased complexity of these assessment tools.[11,15,30] In this work, we present an approach using split GFP to directly assess cargo localization. This approach facilitates optimization of nanogel (NG) polymer composition and surface functionalization for endosomal escape (Scheme 1).[27] While the approach holds promise for many protein cargos, we focused this project on caspases because of their potential for targeted cell killing, in the context of proliferative diseases, including cancer, rheumatoid arthritis, and scleroderma. Furthermore, caspase-3 has been delivered by many materials,[31−37] in addition to our redox-responsive systems,[38,39] underlying merit for this development. The caspase-3 cargo for split GFP developed herein can be utilized to evaluate endosomal escape or, simply, cytosolic concentration, for any system, so long as the system allows release of the cargo protein in the cytosol. Caspases are cysteine aspartate proteases that play a vital role in the initiation and propagation of apoptosis, a form of programmed cell death that allows removal of cells without collateral damage to adjacent cells.[40,41] In contrast to small-molecule cytotoxins that have dangerous implications upon excretion into the environment, as human proteins, caspases are biodegradable, environmentally friendly, and nonimmunogenic. In addition, because caspases are inherently catalytic, they can function at substoichiometric levels.

The principal goal of the work described here has been to develop a method that would allow quantitation of endosomal escape that could guide development of effective cytosolic delivery and enable the direct comparison of various delivery vehicles. Using split GFP to trace cytosolic delivery of casp-3, we have demonstrated herein that endosomal escape: (i) is independent of the extent of protein cargo loaded in the

https://dx.doi.org/10.1021/acs.biomac.0c01767
Biomacromolecules XXXX, XXX, XXX−XXX

nanogels; (ii) is independent of the carrier architecture, that is, whether it is based on block or random copolymers, (iii) is enhanced with cationic and pH-responsive peptides on the surface of the nanocarriers, and (iv) assessed using this methodology can be translated to other delivery systems capable of delivering casp-3.

EXPERIMENTAL SECTION

C3-11 Variant Expression and Purification. Generation of $C3^{KO}$-11 and C3-11 variants have been described previously.[27] pET23b plasmid encoding human WT casp-3, or variant, was transformed into BL21(DE3) *E. coli* cells via electroporation and plated on agar plates containing ampicillin (100 μg/mL). Single colony cultures were grown in 50 mL of LB media with the corresponding antibiotic at 37 °C overnight. The following day 8L of LB was inoculated with ∼5 mL per L of the small seed culture and grown at 37 °C until an OD_{600} of ∼0.6 was achieved. The incubation temperature was then reduced to 25 °C and cells were induced with a final concentration of 0.1 mM isopropyl β-D-1-thiogalactopyranoside (IPTG) and left to express protein for ∼3 h. Cells were then harvested via centrifugation for 10 min at 4700×g and stored at −80 °C. Cell pellets were thawed and lysed using a microfluidizer (Microfluidics, Inc.) in a buffer containing 50 mM Na_3PO_4, 300 mM NaCl, and 2 mM imidazole, pH 8. Lysed cells were centrifuged at 30600×g for 55 min to remove cellular debris. The lysate supernatant was then loaded onto a precharged 5 mL HiTrap Ni-affinity column (GE Healthcare) and the column was subsequently washed with lysis buffer. Following the lysis wash, the column was further washed with an increased imidazole concetration, 50 mM, and the protein was finally eluted using a linear gradient to 300 mM imidazole. The eluted protein was diluted 7-fold in a buffer containing 20 mM Tris and 2 mM DTT, pH 8. This ∼175 mL solution was then loaded onto a 5 mL HiTrap Q column (GE Healthcare) and finally eluted using a linear NaCl steep gradient in 20 mM Tris, 2 mM DTT, pH 8. The Q-fractions were analyzed for purity via SDS-PAGE and concentration concluded via A_{280} absorbance, using molar extinction coefficients ∼25900 M^{-1} cm^{-1} and subsequently stored at −80 °C.

Casp-3 Random Copolymer NG Formation. Casp-3 NG were formulated similar to previous methods.[38] A total of 20 mg of the appropriate random PEG−PDS derivative was added to a vial and dissolved in 1 mL of 1× PBS, pH 7.4, and mixed via sonication for a final concentration of 20 mg/mL polymer. This polymer stock solution was stirred at 4 °C for ∼1 h before 0.5 mL was aliquoted into a new vial. To the 10 mg polymer aliquot, a casp-3 variant solution was added at a weight ratio of 25:1 polymer/protein with additional 1× PBS to achieve a final concentration of 10 mg/mL polymer (or a final volume of 1 mL). The polymer−protein solution was left to stir for ∼3 h at 4 °C. The conjugates were then cross-linked using a concentration of dithiothreitol sufficient for 20−40% cross-linking (0.04 mg) and additional stirring for ∼1 h at 4 °C. An excess of a thiol containing ligand (2 equiv of the remaining PDS groups after cross-linking), such as a cysteine-terminated arginine peptide used herein, was then added and stirred for 2 h. The NG conjugates were then purified via dialysis against 1× PBS pH 7.4 using a 100 kDa MWCO aqueous membrane for ∼20 h at 4 °C with multiple buffer changes. Dialysis against this large membrane allows removal of the cross-linking byproduct, excess ligand, DTT, and unencapsulated protein simultaneously. Prior to dialysis, cross-linking and functionalization were quantified using 2 μL of the NG solution + 98 μL water ± excess DTT and recording the absorbance of the cross-linking byproduct at 343 nm using UV−vis spectroscopy.

Casp-3 Block Copolymer Aqueous NG Formation. Casp-3 NG were formulated by dissolving 5 mg of the appropriate block PEG−PDS derivative in 0.5 mL of 1× PBS, pH 7.4, via sonication for a final concentration of 5 mg/mL polymer, due to polymer solubility limitations. Using constant vortexing and sonication, the polymers took several hours to dissolve in PBS. Next, a casp-3 variant solution was added at a weight ratio of 25:1 polymer/protein with additional 1× PBS to achieve a final concentration of 5 mg/mL polymer. The polymer−protein solution was left to stir for ∼3 h at 4 °C. The conjugates were then cross-linked, functionalized, dialyzed, and characterized as described for the random copolymer NG.

Casp-3 Block Copolymer Cosolvent NG Formation. Casp-3 NG were formulated by dissolving 10 mg of the appropriate block PEG−PDS derivative in 0.1 mL of DMSO (10% of the final volume) via sonication and stirring at room temperature for ∼15 min. To this solution, 0.9 mL of 1× PBS containing the appropriate amount of a casp-3 variant (ratio still 25:1) was added dropwise with stirring at room temperature. This vial was immediately moved to stir for ∼3 h at 4 °C. The conjugates were then cross-linked, functionalized, dialyzed, and characterized, as described for the random copolymer NG.

NG-Mediated Protein Encapsulation and Release. Purified nanogels were removed from dialysis and the volumes were adjusted to be uniform. To visualize protein release, 30 μL of the nanogel solution was incubated with either 10 μL of 1 M DTT or autoclaved water and left for 15 min at RT. Next, 10 μL of SDS-PAGE 3× dye (with reductant) was added to the DTT-NG sample and reductant-free SDS-PAGE 3× dye was added to the water−NG sample. The samples were immediately boiled at 95 °C for ∼5 min and then added to a 16% SDS-PAGE and electrophoresis was executed at 175 V for 60 min. Control protein samples were prepared using 30 μL of 10 μM protein and 10 μL of SDS-PAGE 3× dye, subsequently adding 10, 5, 2.5, and 1.25 μL to the gel, respectively. To compare encapsulation efficiencies, only when run on the same gel, full-length $C3^{KO}$-11 band intensities of different concentrations were assembled into a calibration curve and compared to NG-released $C3^{KO}$-11 using Image Lab Software.

SEE Flow Cytometry Experiments. Two days prior to the assay, HEKs1−10 cells were plated at a density of ∼5 × 10^4 in a 24-well plate and left to adhere for ∼24 h. Upon reaching confluence, cells were treated with purified nanomaterial diluted in a mixture of complete DMEM (Gibco #11965) and 10% v/v 1× PBS, pH 7.4. When chloroquine (CQ) was used, a 100 mM CQ stock was freshly prepared weekly using Milli-Q water. On the day of the experiment, the 100 mM stock was freshly diluted into media (12.5−100 μM) and NG were diluted into these CQ-containing medias. If not specifically mentioned, 100 μM was used. After ∼24 h (unless otherwise noted), the cell incubation media was removed and cells were washed twice with 1× PBS (Gibco, Thermofisher) and incubated with 100 μL of 1× trypsin solution (prepared from 0.5% Trypsin-EDTA, Gibco #15400054) for ∼5 min at 37 °C. 200 μL of FACS buffer (sterile filtered 0.5% BSA in 1× PBS, pH 7.4) was added to the wells, and the entire solution was mixed and then transferred to FACS compatible tubes. Samples were immediately assayed with 488 nm GFP laser line. Samples were analyzed first using a morphological gate (forward scatter-area vs side scatter-area (FSC-A vs SSC-A)) followed by a gate to include only single cells (FSC-A vs forward scatter-height (FSC-H)). Finally, this single-cell population was gated against the media only (untreated, cells only) control to have ∼0.5−1% GFP positive cells (histogram of FITC-A). Percent GFP positive (GFP+) values were reported as quantified by the FlowJo, LLC software. For GFP MFI, samples were normalized to the media-only control. Data were analyzed by one- or two-way ANOVA, with p-values calculated with GraphPad Prism 6.0. Differences were considered statistically significant when $p \leq 0.05$. P-values are illustrated with asterisks, where *$p < 0.05$; **$p < 0.01$; ***$p < 0.001$; ****$p < 0.0001$.

Bafilomycin Treatment. Prior to NG addition to HEKs1−10 cells, cells were treated with bafilomycin (50 nM) containing media for 45 min. Subsequently, bafilomycin media was removed and replaced with fresh bafilomycin-free media in the presence or absence of 80 μM chloroquine. NG were subsequently added and left to incubate for 24 h before SEE analysis.

Protein Modification with Boronic Acid Linkers for Inclusion in MSi NP. A total of 120 μL of $C3^{KO}$-11 (123 μM, 0.46 mg), 200 μL of H_2O, and 40 μL of $NaHCO_3$ solutions (0.5 M) were dissolved in a 5 mL vial under stirring at room temperature. To the vial, 10 μL of DMSO solution containing 1.5 mg of linker **1** or 2 mg of linker **2** was added (Figure S13). The reaction mixture was then

https://dx.doi.org/10.1021/acs.biomac.0c01767
Biomacromolecules XXXX, XXX, XXX−XXX

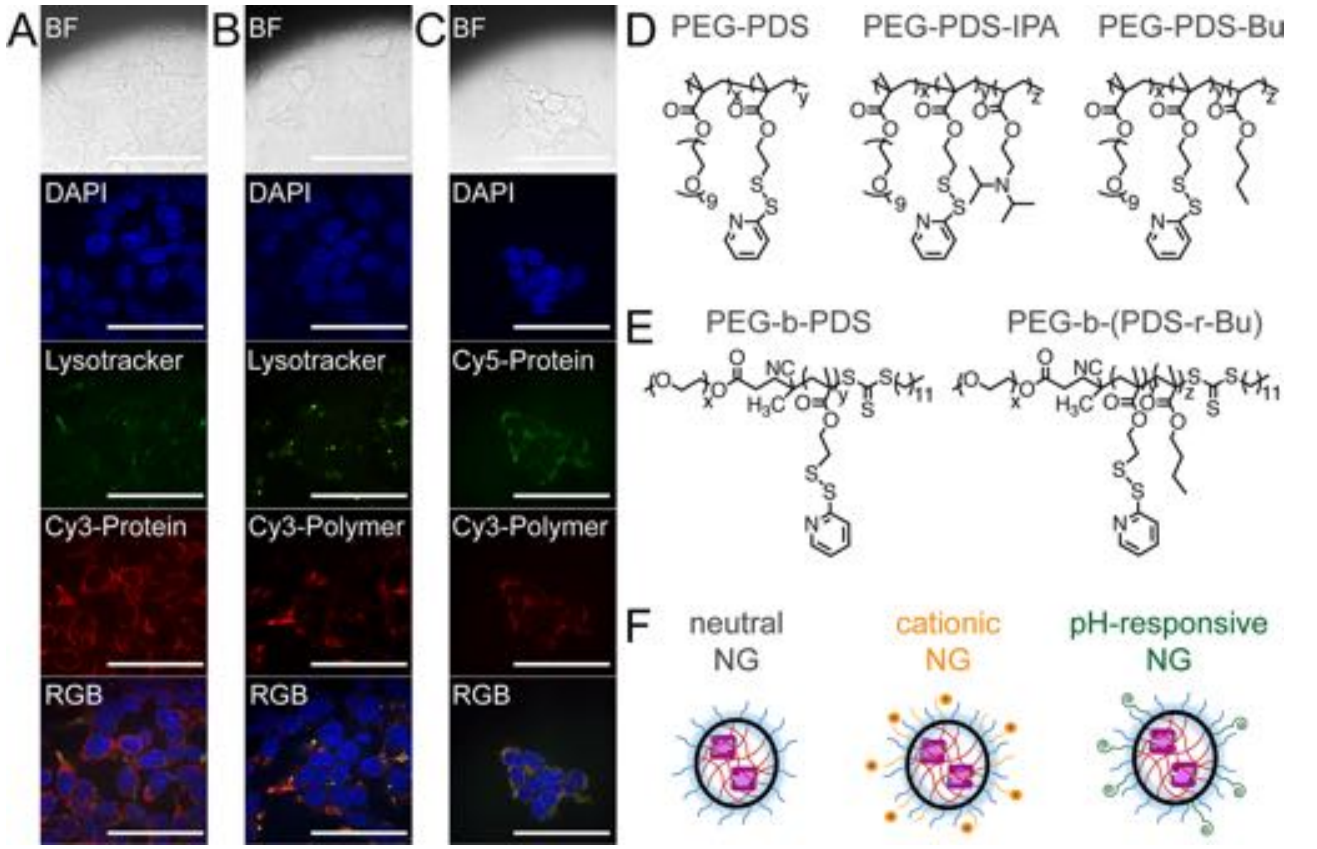

Figure 1. PDS containing polymers deliver casp-3 via endocytosis. Confocal fluorescence microscopy of the (A) Cy3-$C3^{KO}$-11 protein delivered by unlabeled NG. (B) Cy3−PEG−PDS NG delivering unlabeled $C3^{KO}$-11. (C) Cy3−PEG−PDS NG delivering Cy5-$C3^{KO}$-11. HEK293T cells, 60× objective, BF (bright-field), DAPI (nucleus stain, 405 nm), Lysotracker (acidic endosomal stain, 488 nm), Cy3 (532 nm), and Cy5 (632 nm). Scale bars indicate 80 μm. (D) Random copolymer structures of poly(ethylene glycol) and pyridyl disulfide (PEG−PDS) derivatives. (E) Block copolymer structures. (F) Representation of nanogels (NGs) with varying surface functionalities.

stirred at room temperature for an additional 6 h, followed by ultrafiltration purification with Amicon Ultra Centrifugal Filters (MWCO = 3 kDa) for 5 times. The final modified protein was dissolved in 230 μL of distilled DI water (2 mg/mL) and stored at −20 °C.

RESULTS AND DISCUSSION

Redox-responsive polymers provide many promising characteristics for caspase delivery including a stealth material, postmodification capability, efficient protein encapsulation, reductant-induced traceless protein release, and cargo-induced cell death.[38,42] We previously generated and characterized a casp-3 variant capable of cytosolic tracking using split GFP complementation. Specifically, casp-3 was tagged with the 11th strand of GFP containing three solubilizing mutations, which we refer to as C3-11 (also called C3-11^{M3} but referenced here as C3-11 for simplicity). C3-11 maintains properties of native casp-3 and can report on cytosolic localization upon reassembly with GFP1−10, which is constitutively expressed cytosolically (Scheme 1).[27] We often used a catalytically dead variant generated by knocking out (KO) the active site cysteine residue generating $C3^{KO}$-11.[27] Using this catalytically dead variant allowed us to track cytosolic levels of casp-3 without inducing apoptosis. Nevertheless, $C3^{KO}$ should mimic an active casp-3 therapeutic cargo in polymer−protein formulation, nanoparticle uptake, and resultant translocation.

Casp-3 was delivered by random copolymers composed of poly(ethylene glycol) (PEG) and pyridyl disulfide (PDS), termed PEG−PDS.[38] Cross-linked PEG−PDS NG demonstrate excellent stability of noncovalently and covalently encapsulated guests, a small molecule or protein, in both the absence[43−45] and presence[46] of serum. A significantly punctate distribution[38] was visualized upon microscopy, which is often taken to be consistent with endosomal entrapment. This was true, independent of whether the protein (Figure 1A) or polymer (Figure 1B) is fluorescently labeled. Accordingly, imaging of dual-labeled NG (Cy3-polymer, Cy5-protein) demonstrates punctate colocalization of the cargo and delivery vehicle (Figure 1C), implying great complex internalization. Despite this endosomal entrapment, it is clear that the amount of casp-3 that does escape the endosome is sufficient to induce cell death,[27,38] but enhancing endosomal escape is a warranted investigation to optimize efficacy.

To determine if polymer structure could significantly improve endosomal escape, we generated a series of linear polymer derivatives with varying compositions and architectures. All of the polymers evaluated herein maintained the PDS group necessary for casp-3 encapsulation and traceless release (Figure S1), but have alterations in particle charge or hydrophobicity. Our group has previously synthesized PEG−PDS with random incorporation of diisopropylamino moieties (IPA), PEG−PDS−IPA.[44] We hypothesized that PEG−PDS−IPA (Figure 1D) may afford better endosomal escape than PEG−PDS, as PEG−PDS−IPA demonstrates an increase in zeta potential upon decreased pH.[44] To understand the effect of increasing polymer hydrophobicity, PEG−PDS with butyl

https://dx.doi.org/10.1021/acs.biomac.0c01767
Biomacromolecules XXXX, XXX, XXX−XXX

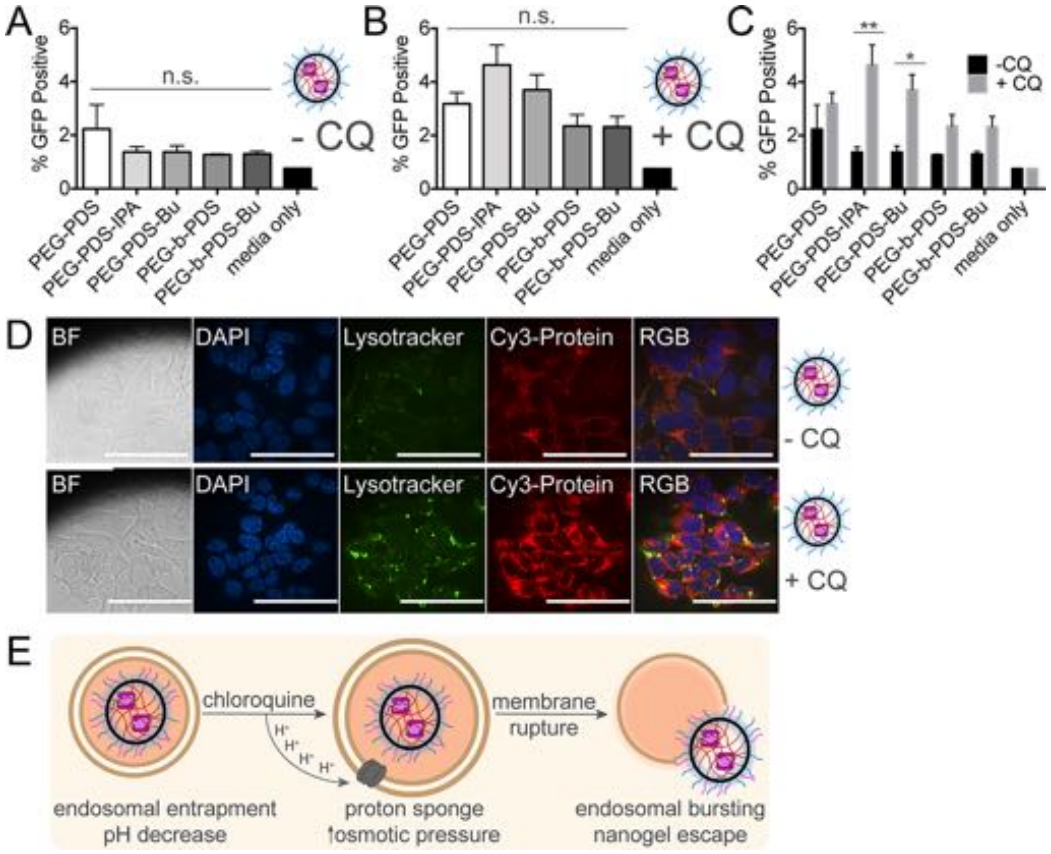

Figure 2. Incorporation of isopropyl amine or butyl functionalities within PEG−PDS polymers has little influence on C3^{KO}-11 SEE. (A) SEE after a 24 h incubation with nanogel (NG) complexes at 0.75 mg/mL polymer concentration in HEKs1−10 cells demonstrates the little influence of the polymer structure on endosomal escape. Measured by split GFP, endosomal escape is quantified as GFP positive cells (Ex. 488 nm). Untreated, single-cell HEKs1−10 population is gated for baseline GFP fluorescence levels, and any cell beyond the gate is categorized as GFP positive. SEM error bars pertain to individual biological replicates from independent NG batches, analyzed on different days. (B) NG complexes, in the presence of 80 μM chloroquine diphosphate (CQ), show an increased GFP positive population. (C) NG complexes demonstrated differences in GFP positive cell significance, with and without CQ. (D) Confocal microscopy of NG (Cy3-C3^{KO}-11 protein) in HEK293T cells; 60× objective, BF (bright-field), DAPI (nucleus stain, 405 nm), Lysotracker (acidic endosomal stain, 488 nm), Cy3 (532 nm), scale bars indicate 80 μm. (E) Hypothesized proton sponge mechanism of chloroquine-mediated endosomal disruption, liberating NG entrapment in endosomes. SEM error bars pertain to four or more individual biological replicates from independent NG batches analyzed on different days. (A, B) One-way ANOVA was performed against PEG−PDS, no significant (n.s.) differences found. (C) Two-way ANOVA was performed, where *$p < 0.05$; **$p < 0.01$; ***$p < 0.001$; ****$p < 0.0001$. If no label present, no significant (n.s.) differences found.

(Bu) moieties, PEG−PDS−Bu, were also synthesized (Figure 1D). As changes in particle size, rigidity, and hydrophobics have been shown to influence cellular internalization,[47−49] we also aimed to change the hydrophilic−hydrophobic positioning by using block copolymers of PEG−PDS and PEG−PDS−Bu, termed PEG-*b*-PDS and PEG-*b*-(PDS-*r*-Bu), respectively (Figure 1E). To assess the importance of the hydrophobic component, Bu composing 25% of the hydrophobic block (PEG-*b*-PDS-Bu$_{25}$) or 40% (PEG-*b*-PDS-Bu$_{40}$) were compared. In addition, the effect of NG surface functionalization by cationic or pH-sensitive moieties was also explored (Figure 1F). PEG−PDS NGs can easily be functionalized via PDS substitution, with any ligand containing an available thiol (Figure S1).[38]

To track endosomal escape of casp-3, we developed a split-complementation endosomal escape (SEE) assay. Casp-3 tagged with GFP11 (C3^{KO}-11)[27] was delivered by NG into HEKs1−10, which are HEK cells stably expressing the other 10 β-strands of GFP (GFP1−10).[50] Following endocytosis and subsequent endosomal escape, high cytosolic glutathione (1−10 mM)[51,52] mediates NG-disassembly, liberating C3^{KO}-11 from the NG to reassemble with GFP1−10.[27] PEG−PDS−IPA and PEG−PDS−Bu polymers maintained the ability to encapsulate and release C3^{KO}-11 from NG, although the encapsulation efficiency by PEG−PDS was consistently higher (Figure S2). Furthermore, the three polymers delivered comparable levels of C3^{KO}-11 overall (Figure S2). Nevertheless, upon first assessment of NG delivered C3^{KO}-11, no significant GFP signal was observed, regardless of the polymer used (Figure 2A). As endosomal escape is an extremely inefficient process, a lack of GFP signal can be attributed to low levels of escape or these data may hinge on sensitivity limitations. It has recently been reported that biological concentrations above 10 μM are required to observe split GFP-mediated endosomal escape in cells.[53]

Alternative strategies to improve NG-mediated endosomal escape were undertaken as the next step of development of an optimal casp-3 delivery vehicle. NG doses were titrated up to 2 mg/mL, and the time required for both NG incubation and cellular reassembly of the GFP fragments were monitored (8−48 h). As expected, the GFP signal increased with increased incubation time, but otherwise, no significant improvements

https://dx.doi.org/10.1021/acs.biomac.0c01767
Biomacromolecules XXXX, XXX, XXX−XXX

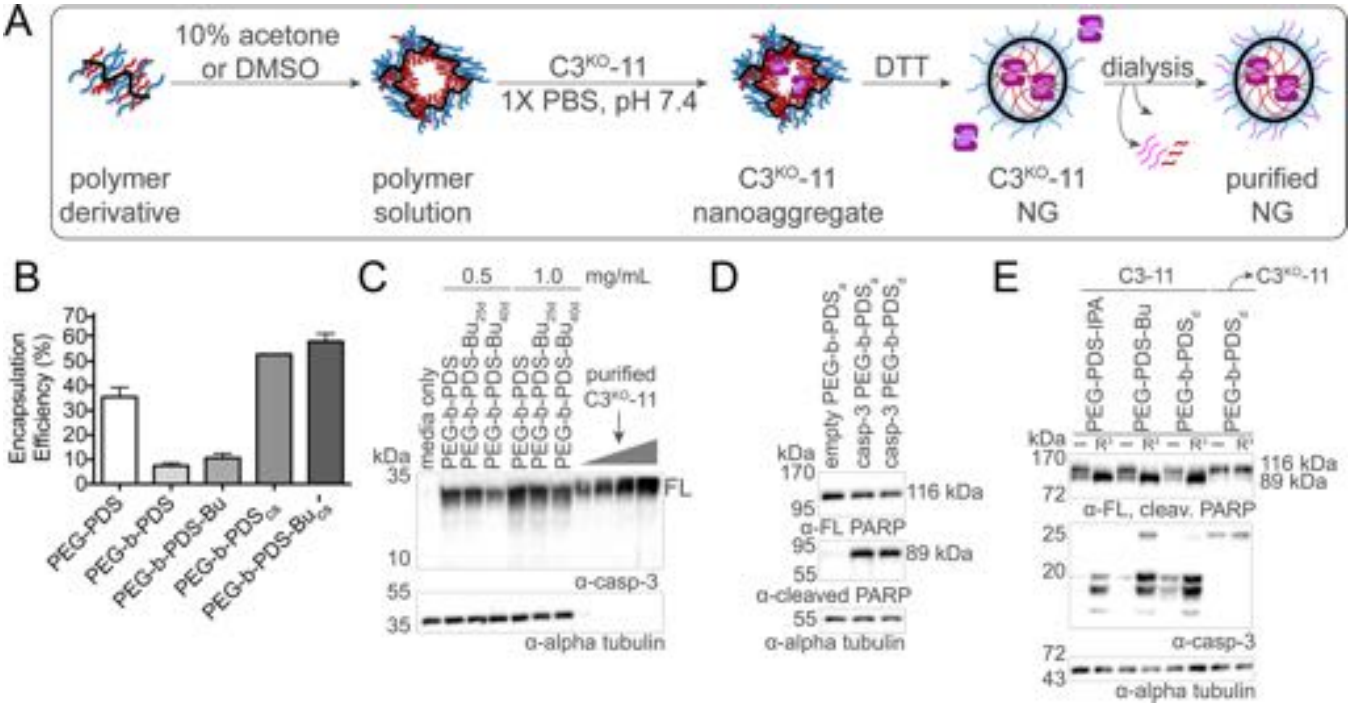

Figure 3. Cosolvent block copolymer NG formation. (A) Cosolvent block copolymer nanogel (NG) formation begins by dissolving the polymer in solvent, followed by the dropwise addition of an aqueous solution containing $C3^{KO}$-11 with stirring. The general NG encapsulation, cross-linking and purification procedure is then followed. (B) Encapsulation efficiencies of the block copolymers are enhanced by the cosolvent methodology (cs subscript). (C) Visualization of PEG-*b*-PDS NG-mediated delivery of $C3^{KO}$-11 to MCF7 cells at two different doses (1.0 and 0.5 mg/mL polymer concentration). Purified $C3^{KO}$-11 was added at 0.2, 0.4, 0.8, and 1.6 μg/mL. (D) PEG-*b*-PDS NG prepared using cosolvents acetone (a subscript) or DMSO (d subscript) mediated delivery of WT casp-3 demonstrated cleavage of poly(ADP-ribose) polymerase 1 (PARP), indicating delivery of active casp-3 WT and apoptosis, with an empty NG control prepared using the cosolvent methodology. (E) Delivery of active C3-11 by PEG−PDS NG derivatives, unfunctionalized (−) and Arg^3 (R^3) functionalized, and resultant PARP cleavage. These data demonstrate the ability of $C3^{KO}$-11 to maintain activity against apoptotic substrates in cells and that R^3 functionalization increased total protein delivered and subsequently increased the resultant PARP cleavage for various NG. Delivery of inactive $C3^{KO}$-11 used as control to demonstrate a lack of apoptosis from an inactive casp-3 cargo.

were observed. Endosomal-buffering agents, such as chloroquine diphosphate (CQ), can liberate NG trapped in endosomes.[27] Notably, CQ has been shown to mitigate challenges beyond endosomal escape, such as decreasing nanoparticle immunological clearance and increasing cytotoxic therapeutic efficacy in cancer tissues.[54] Accordingly, the use of CQ in the evaluation of delivery systems has become increasingly prevalent as CQ largely increases delivery system efficiency via the proton sponge effect.[55−58] Upon protonation, CQ neutralizes the acidification of endosomes, preventing endosomal−lysosomal fusion and inducing osmotic swelling, leading to vesicle rupture.[59,60] In these studies, CQ is a useful chemical tool because, when combined with data analyzing total delivered protein content, it can allow the calculation of the ratio of uptake to endosomal escape. Upon the addition of CQ (80 μM), we observed a slight increase in the total percentage of GFP positive cells (Figure 2B). The highest increase observed upon the addition of CQ was induced by PEG−PDS−IPA, followed by PEG−PDS−Bu (Figure 2C). As PEG−PDS, PEG−PDS−IPA, and PEG−PDS−Bu delivered similar levels of protein overall (Figure S2), these data imply that PEG−PDS−IPA may be increasing the number of NG per endosome, yet, the IPA moieties are insufficient at inducing significant escape through a proton-sponge mechanism without CQ. CQ-induced changes in vesicle number and volume were visualized using an endosomal marker, consistent with the expected CQ-mediated vesicle swelling (Figure 2D). We ensured that the addition of CQ did not meaningfully favor the total amount of protein delivered (Figure S3) or the total amount of polymer delivered (Figure S4). These data strongly indicate that CQ herein is acting on endosomal escape, not uptake, through the proton sponge mechanism (Figure 2E).

To determine whether the total amount of cytosolic casp-3 could be enhanced by increasing protein encapsulation within the NG, we altered the protein−polymer assembly strategy for the block copolymers. Traditionally, PEG−PDS random copolymer NG assemblies demonstrated encapsulation efficiencies of approximately 30 wt % (Figure S2). Comparatively, block copolymer casp-3 assemblies demonstrated notably lower amounts of encapsulation with minimal cellular uptake observed upon immunoblot analysis (Figure S5). The lower encapsulation efficiencies of the block copolymer may be due to a preformed dense and difficult-to-penetrate polymeric core. To increase dynamics within the block copolymer aggregates and enhance protein−polymer reactivity, we explored cosolvent formulations.[48] We selected dimethyl sulfoxide (DMSO), known to be compatible with casp-3 activity at low concentrations (>8%), and the volatile solvent acetone as two cosolvents for block copolymer−protein assemblies, denoted with a subscript for the cosolvent: PEG-*b*-PDS_d and PEG-*b*-PDS_a, respectively. Cosolvent $C3^{KO}$-11 NG formation begins by dissolving the polymer in the organic solvent. Casp-3 in aqueous buffer is then added to the polymer dropwise, followed by normal NG cross-linking and purification

https://dx.doi.org/10.1021/acs.biomac.0c01767
Biomacromolecules XXXX, XXX, XXX−XXX

procedures (Figure 3A). Protein release, monitored by SDS-PAGE analysis (Figure S6), demonstrated an increase in block copolymer encapsulation efficiency from approximately 10% to 40% using the cosolvent methodology, compared to the aqueous formulation strategy (Figure 3B). Fittingly, effective intracellular delivery of casp-3 was demonstrated by immunoblot analysis of total cell lysates (Figure 3C) at levels of 0.48 ± 0.21 μg/mL (0.5 mg/mL NG dose) and 0.69 ± 0.11 μg/mL (1.0 mg/mL NG dose). Thus, it is clear that increasing casp-3 cargo loaded into NG delivery vehicles increases the intracellular casp-3 titer that can be achieved.

The cosolvent-assembled block copolymers can be therapeutically impactful only if casp-3 retains activity upon encapsulation. To ensure that cosolvents did not prevent the ability of $C3^{KO}$-11 to generate GFP fluorescence for SEE, we tested NG-released reassembly. Released $C3^{KO}$-11 demonstrated robust fluorescence in the presence of GFP1−10 (data not shown), demonstrating that DMSO-mediated encapsulation did not negatively impact split GFP reassembly. Furthermore, to ensure that cosolvent encapsulation did not irreversibly denature or otherwise inactivate casp-3, we encapsulated active WT casp-3 in block copolymer NGs, which should activate apoptosis and result in poly(ADP-ribose) polymerase 1 (PARP) cleavage[61,62] if cosolvent encapsulated WT casp-3 remained active. Cosolvent block copolymer casp-3 NG delivery resulted in a significant disappearance of full-length PARP and appearance of cleaved PARP, indicating that active casp-3 was effectively delivered in both accounts. In contrast, no significant apoptosis-induction was induced from empty NG prepared using cosolvent methodologies (Figure 3D). Likewise, delivering the active casp-3 variant capable of reassembling split GFP (C3-11)[27] in aqueous random or cosolvent block formulations again displayed significant PARP cleavage (Figure 3E). Together these results suggest that both aqueous and cosolvent formulations allow delivery of active casp-3.

Despite the increased casp-3 encapsulation efficiencies in the block copolymer assemblies, levels of SEE-mediated fluorescence were identical to aqueous formulations. These data suggest that endosomal escape rates are better for the aqueously formulated block copolymer NG, since the same number of casp-3 molecules would be contained in a greater number of aqueous NG. We reasoned that addition of surface functionalization that could increase uptake or endosomal escape could increase cytosolic delivery of casp-3. In line with that prediction, NGs functionalized on the surface with a triarginine peptide (R^3) demonstrated higher levels of both casp-3 delivery and subsequent PARP cleavage (Figure 3E). Given this result, we next investigated the effect of cationic surface functionalization on SEE.

Guanidine and other positively charged moieties on the surface of delivery vehicles increase membrane-association, permit cell entry through endocytosis, and aid in endosomal escape.[63−66] Our group has utilized varying cationic moieties, such as arginine-repeat peptides[38,43,67] or TAT,[68] to functionalize the NG surface, allowing for the addition of surface-exposed guanidine groups. To assess the impact of surface-functionalization on casp-3 delivery, $C3^{KO}$-11 PEG−PDS NGs were functionalized via thiol exchange (Figure S1) with PEG-amine, arginine peptides of various lengths (R^3, R^6, R^9) or TAT (Figure S7).[38] Fortunately, in addition to spectroscopic assessment, reductant-mediated release of higher degree oligopeptides can be observed by SDS-PAGE analysis (Figure S7). To ensure identical protein encapsulation and cross-linking, NGs were always prepared as a large batch prior to functionalization, which resulted in similarly sized NGs for postfunctionalization (Figure S7).

Following treatment of cells with Arg-functionalized NG, we observed a 3- to 6-fold increase in the number of GFP-positive cells due to SEE (Figure 4A), relative to unfunctionalized NG, strongly suggesting that cationic NGs promote endosomal escape. Upon the addition of CQ, cationic functionalized NGs demonstrated an additional 4- to 13-fold increase in GFP

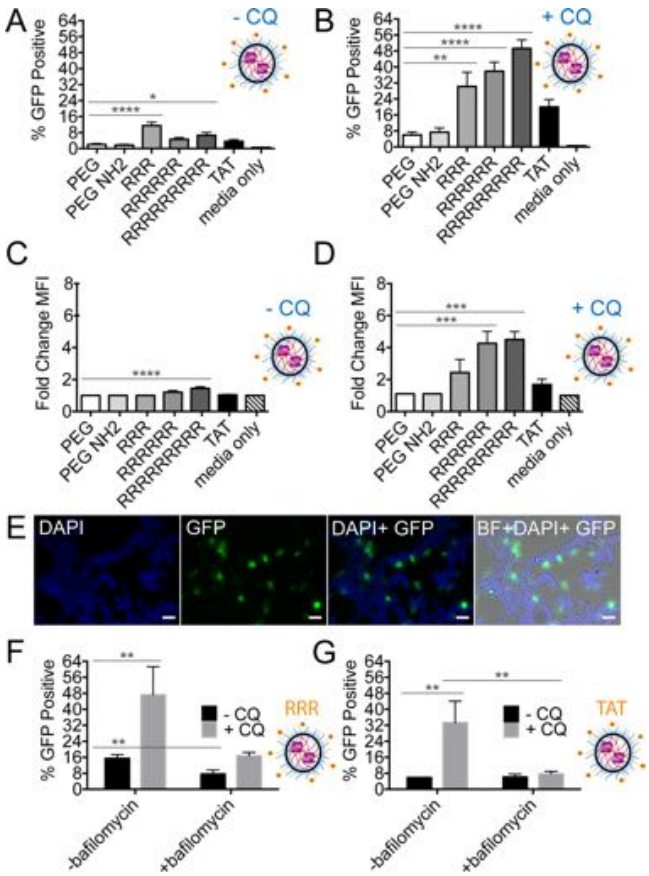

Figure 4. NG functionalization with cationic peptides enhances endosomal escape. (A) SEE after 24 h incubation with surface-modified PEG−PDS NG complexes at 0.75 mg/mL polymer concentration in HEKs1−10 cells indicates that Arg-functionalization aids in endosomal escape. SEM error bars pertain to individual biological replicates from independent NG batches, analyzed on different days. (B) In the presence of 80 μM CQ, a significant increase in fluorescence was observed, suggesting that Arg-functionalization may also increase the number of NG within endosomes. (C) SEE represented as change in GFP mean fluorescent intensity (MFI) of cells in CQ-free media. The change in MFI is generated after normalizing GFP MFI to the untreated, viable single-cell HEKs1−10 population. (D) In the presence of 80 μM CQ. (E) Visualization of CQ-liberated endosomes after 24 h incubation with R^3−PEG−PDS NG (20× objective: BF (bright-field), DAPI (nucleus stain, Ex. 405 nm), GFP (reassembly of $C3^{KO}$-11 and GFP1−10, Ex. 488 nm), scale bar indicates approximately 50 μm). (F) SEE of R^3−PEG−PDS NG and (G) TAT−PEG−PDS NG with and without CQ and bafilomycin, an endosomal acidification inhibitor. (A−D) One-way ANOVA performed against PEG−PDS, where *$p < 0.05$; **$p < 0.01$; ***$p < 0.001$; ****$p < 0.0001$. If no label present, no significant (n.s.) differences were found. (F, G) Individual unpaired t tests were performed.

https://dx.doi.org/10.1021/acs.biomac.0c01767
Biomacromolecules XXXX, XXX, XXX−XXX

signal compared to nonfunctionalized NGs in the presence of CQ (Figure 4B). In the absence of CQ, we observed a 1.2−1.4-fold increase in the GFP mean fluorescence intensity (MFI) (Figure 4C). Although minimal, this increase was evident, as we previously observed no significant GFP positive population for the nonfunctionalized NG and correspondingly, no change in MFI. However, the addition of CQ significantly increased the GFP MFI further, 2.4−4.5-fold (Figure 4D). Due to the effects of CQ, we hypothesize that this increase could be attributed to Arg-mediated increases in the concentration of NGs per endosome. However, we cannot rule out the possibility there may also be more endosomes to accommodate increased numbers of NG.[28] CQ-liberated endosomally entrapped R^3-NG were also readily visualized by microscopy (Figure 4E, Supporting Information, Figure S8). In summary, arginine-functionalized caspase-containing NG demonstrated enhanced endosomal escape, although the results with CQ imply that a significant population of NGs still remain trapped in endosomes. Therefore, as noted for other delivery systems,[23,24] arginine moieties enhance the general uptake, but these data demonstrate that arginine can also directly enhance endosomal escape, although not necessarily to 100% of the NG particles uptaken. To further probe the uptake mechanism, bafilomycin, an ATPase inhibitor that prevents endosomal acidification, was applied to NG-treated cells.[52,69,70] SEE was significantly decreased in the presence of bafilomycin for R^3-NG (Figure 4F), in the absence or presence of CQ. SEE was also decreased for TAT-NG (Figure 4G), underscoring our assertion that arginine protonation and CQ influences endosomal escape through the proton sponge effect.[63]

Having shown that NG surface functionalization influences translocation, we reasoned that improved delivery may be achievable by exploiting the inherent pH decrease upon early-to-late endosomal processing. To date, surface modifications of polymeric NG with peptides capable of pH-responsive conformational changes has yet to be investigated. Importantly, pH-responsive functionalities are hypothesized to permit endosomal escape through mechanisms beyond the proton sponge alone, that is, via a combination of rapid osmotic swelling and membrane destabilization, leading to endosomal rupture.[71−73] Inspired by the *N*-terminal anionic domain of an influenza virus protein, synthetic pH-sensitive peptides composed of varying glutamic and aspartic acid residues have been generated to explore their membrane-disrupting properties.[12,74] GALA, a 30-mer glutamic acid−alanine−leucine−alanine repeat, and KALA, a cationic derivative composed of lysine−alanine−leucine−alanine repeats, have been applied to enhance endosomal escape of cationic liposomes, cationic polymers, and antibodies.[12,75] Due to their length and hydrophobicity, truncated versions of these peptides,[76] as well as another peptide based on the endodomain of the HIV enveloped glycoprotein gp41, termed HGP,[77,78] can be more easily used. We incorporated GALA, KALA, and HGP onto the surface of our nanogels by adding a *C*-terminal cysteine to the peptides[74,78−81] for reaction with PEG−PDS (Figure S9). SEE analysis demonstrated that only functionalization with KALA resulted in significant GFP signal, independent of CQ (Figure 5A). These data suggest that the combination of pH-responsive and cationic properties by KALA afford more endosomal escape than the pH-responsive properties alone in GALA and HGP. As mentioned above, often the enhancement of endosomal escape is compromised due to the toxicity associated with these peptides, which was observed for KALA

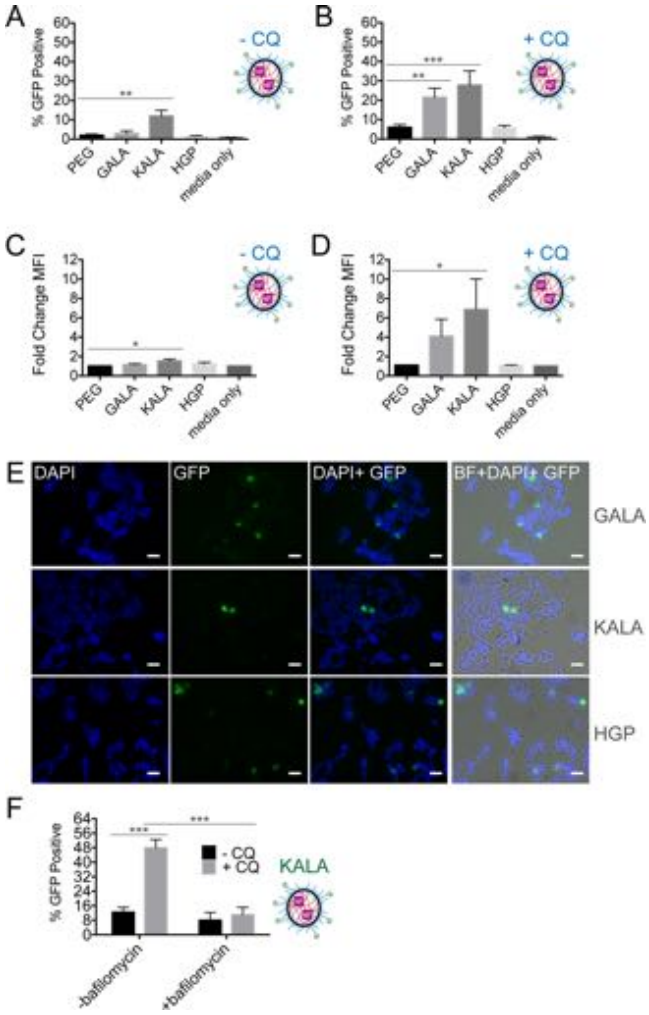

Figure 5. NG functionalization with pH-sensitive peptides influences endosomal escape. (A) SEE after a 24 h incubation with surface-modified PEG−PDS NG complexes at 0.75 mg/mL polymer concentration in HEKs1−10 cells and (B) in the presence of 80 μM CQ. SEM error bars pertain to individual biological replicates from independent NG batches, analyzed on different days. (C) SEE represented as change in GFP mean fluorescent intensity (MFI) of cells in CQ-free media. The change in MFI is generated after normalizing GFP MFI to the untreated, viable single-cell HEKs1−10 population. (D) In the presence of 80 μM CQ. (E) Visualized CQ-liberated endosomes after a 24 h incubation with different pH-responsive-NG (20× fluorescent microscope objective: BF (bright-field), DAPI (nucleus stain, 405 nm), GFP (reassembly of $C3^{KO}$-11 and GFP1−10, 488 nm)). SEM error bars pertain to four individual biological replicates from independent NG batches analyzed on different days. (F) SEE of KALA−PEG−PDS NG, with and without CQ and bafilomycin, an endosomal acidification inhibitor. (A−D) One-way ANOVA performed against PEG−PDS, where $*p < 0.05$; $**p < 0.01$; $***p < 0.001$; $****p < 0.0001$. If no label present, no significant (n.s.) differences were found. (F) Individual unpaired *t* tests were performed.

at high degrees of functionalization (Figure S10). Halving the dose of KALA-NG decreased the induced cellular debris (cell death), but correspondingly decreased the subsequent amount of GFP fluorescence observed (17% GFP positive at 1 mg/mL dose vs 5% GFP positive at 0.5 mg/mL dose). These data suggest that the NG dose influenced the amount of NG per endosome. GALA and HGP NG appear to remained trapped until endosome acidification. We observed a significant

https://dx.doi.org/10.1021/acs.biomac.0c01767
Biomacromolecules XXXX, XXX, XXX−XXX

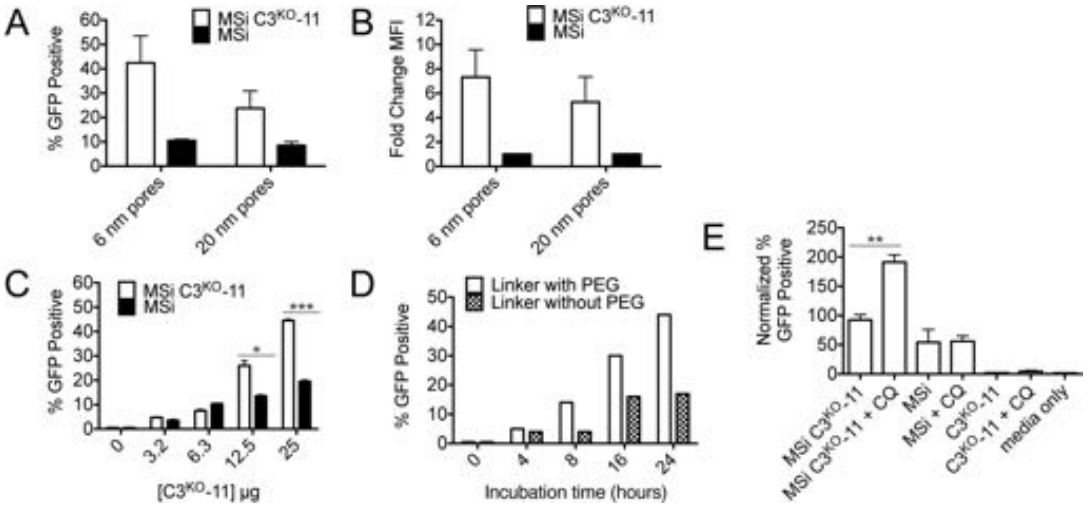

Figure 6. Detecting cytosolic delivery of $C3^{KO}$-11 via mesoporous silica (MSi) nanoparticles by SEE. (A) Influence of MSi pore size on SEE after a 24 h incubation with MSi complexes in HEK293T cells transfected with GFP1−10 and (B) change in MFI. (C) Dose dependence of SEE after a 24 h incubation with MSi complexes in HEKs1−10 cells. (D) Effect of incubation time on SEE. (E) SEE improvement of various MSi complexes in the presence of 100 μM CQ. (C) Two-way ANOVA performed and (E) unpaired t test (two-tailed) executed, where *$p < 0.05$; **$p < 0.01$; ***$p < 0.001$; ****$p < 0.0001$. If no label present, no significant (n.s.) differences were found. (F) Individual unpaired t tests were performed.

increase in GFP positive cells (Figure 5B) and fold change in GFP fluorescence (Figure 5C, 5D) upon the addition of CQ, which could subsequently be visualized by microscopy (Figure 5E and Supporting Information, Figure S11). As pH-responsive moieties may be facilitating endosomal escape through a proton sponge effect, we assayed KALA-NG in the presence of bafilomycin. We found a statistical significance between KALA-NG, with and without CQ, as well as KALA-NG with CQ, with and without bafilomycin, but did not find significance for KALA-NG with and without bafilomycin (Figure 5F). Interestingly, GALA and HGP demonstrated a clear functionalization-dependent response with CQ (Figure S12), confirming that there is still significant endosomal entrapment. These data may suggest that the extent of GALA and HGP functionalization influences the amount of NG per endosome or that higher amounts of these functionalities may work additively with CQ.

A major goal of this work has been to develop a method that allows a robust comparison of delivery vehicles with disparate chemical properties. For this reason, we included in our analysis a delivery vehicle with dramatically different chemical characteristics, mesoporous silica (MSi) nanoparticles. We had previously developed MSi nanoparticles that effectively escape the endosome.[82] To prepare casp-3-congugated MSi, lysine residues on $C3^{KO}$-11 were functionalized with redox-responsive linkers capable of self-immolation (linker structure, Figure S13) for the traceless release of $C3^{KO}$-11. These redox-responsive linkers contain a disulfide, PEG, and a terminal aryl boronic acid moiety (Figure S13, linker structure 2). MSi-protein attachment is achieved through dative bond formation of the boronic acid functionalized protein and amine functionalized MSi.[82] Efficient endosomal escape by MSi is hypothesized to be due to the proton sponge effect, as dissociation between the protein and MSi facilitates exposure of the amine group on MSi surface.[29,63] Accordingly, MSi facilitated effective protein delivery of $C3^{KO}$-11 to MCF7 cells, visible by immunoblot (Figure S13). In both HEK293T cells transfected with GFP1−10 and HEKs1−10, MSi also demonstrated effective casp-3-dependent GFP signal by SEE (Figure 6). MSi with smaller pore sizes demonstrated greater GFP positive populations (Figure 6A), with 7-fold change in GFP fluorescence (Figure 6B), compared to MSi with larger pore sizes. The evolution of the GFP signal can be observed in a dose-dependent manner (Figure 6C) and as a function of time (Figure 6D). Interestingly, it appears that removal of the PEG spacer from the redox-responsive linker (Figure S13, linker structure 1) comparably decreased the GFP signal (Figure 6D), perhaps due to limiting GSH accessibility to the disulfide within the linker. Finally, the MSi-mediated SEE signal doubles upon the addition of CQ (Figure 6E), indicating that some MSi remain trapped in endosomes. These data demonstrate that $C3^{KO}$-11 delivery can be translated to other delivery systems with a range of assembly chemistries, permitting a direct comparison of the resultant cytosolic protein levels by different nanomaterials. Hence, MSi-mediated delivery of $C3^{KO}$-11 resulted in higher cytosolic $C3^{KO}$-11 levels than both unfunctionalized and functionalized polymeric NG, in the absence of CQ. Furthermore, we hypothesize that we can extrapolate the extent of "change" due to CQ as an indicator of the percentage of nanomaterial entrapment. The number of GFP positive cells from MSi $C3^{KO}$-11 increased only 2-fold in the presence of CQ (Figure 6E), while functionalized polymeric NG delivering $C3^{KO}$-11 increased over wider ranges, ∼4−7-fold upon cationic functionalization (Figure 4B) and ∼3−7-fold for pH-responsive functionalization (Figure 5B). These data may indicate that only half of MSi $C3^{KO}$-11 complexes are entrapped, leaving half of the uptaken material to reach the cytosol for therapeutic effect. On the other hand, these calculations imply that only 25−33% of the polymeric materials may reach cytosol, leaving ∼67−80% of the engulfed material endosomally entrapped. Correspondingly, we hypothesize that MSi-mediated delivery of active casp-3 would likewise induce higher levels of cell death, a planned future investigation.

CONCLUSIONS

Known caspase properties, such as their catalytic ability to induce and propagate apoptosis through rapid cleavage of

https://dx.doi.org/10.1021/acs.biomac.0c01767
Biomacromolecules XXXX, XXX, XXX−XXX

other procaspases and cellular substrates, suggest that low levels of cytosolic casp-3 would be sufficient to achieve effective cell death. Prior to this work, we lacked a robust method to estimate the amount of delivered casp-3 that reached the cytosol. Herein we utilized $C3^{KO}$-11, capable of reassembly with GFP1−10, to generate fluorescence and report on casp-3 cytosolic localization in cells. SEE allowed effective monitoring of only cytosolic protein levels after endosomal escape and, importantly, lacked false positive results.

SEE was instrumental in evaluating the role of polymer composition and NG surface functionality in cytosolic delivery. In the field of cell death, the precise level of caspase activation required to induce apoptosis has not been quantified. Undertaking these studies, we anticipated that this approach would allow quantification of the threshold level of active casp-3 required for apoptosis. We were surprised to observe that the levels of casp-3 required to trigger apoptosis induction were so low that even a sensitive technique like SEE was not effective at quantification, indicating that the threshold casp-3 activation levels must be less than 10 μM.[53] Nevertheless, we did observe that increasing protein cargo encapsulation efficiencies within NGs did not enhance SEE, while we know that changing the protein cargo's sequence can influence SEE.[27] Consistent with this effect, changing NG surface-functionalization demonstrated significant improvements, while altering delivery vehicle architecture did not. Thus, the low fluorescence signal from nonfunctionalized NG SEE contributes to the conclusion that (i) SEE is not sensitive enough to detect very low levels of nonfunctionalized NG endosomal escape and (ii) the amount of endosomal escape truly occurring without functionalization or lysosomotropic agents is low. Importantly, this method allows a direct comparison of commonly used approaches, such as cationic functionalization, to increase the amount of delivered protein that reaches the cytosol. Furthermore, we can compare the efficiency of different delivery vehicles that vary by composition, surface functionalization, and cargo tagging methodology by a signal generated solely from the cytosolic protein cargo.

■ ASSOCIATED CONTENT

Supporting Information

The Supporting Information is available free of charge at https://pubs.acs.org/doi/10.1021/acs.biomac.0c01767.

Materials and methods for synthesis and characterization of polymers, as well as procedures for NG characterization (DLS, protein encapsulation and release, immunoblotting, additional microscopy photos), silica synthesis, and protein encapsulation; Figures S1−S13 (PDF)

■ AUTHOR INFORMATION

Corresponding Authors

Jeanne A. Hardy − *Department of Chemistry and Center for Bioactive Delivery at the Institute for Applied Life Sciences, University of Massachusetts, Amherst, Massachusetts 01003, United States;* orcid.org/0000-0002-3406-7997; Email: hardy@chem.umass.edu

S. Thayumanavan − *Department of Chemistry and Center for Bioactive Delivery at the Institute for Applied Life Sciences, University of Massachusetts, Amherst, Massachusetts 01003, United States;* orcid.org/0000-0002-6475-6726; Email: thai@chem.umass.edu

Authors

Francesca Anson − *Department of Chemistry, University of Massachusetts, Amherst, Massachusetts 01003, United States*

Bin Liu − *Department of Chemistry, University of Massachusetts, Amherst, Massachusetts 01003, United States;* orcid.org/0000-0003-1736-9392

Pintu Kanjilal − *Department of Chemistry, University of Massachusetts, Amherst, Massachusetts 01003, United States*

Peidong Wu − *Department of Chemistry, University of Massachusetts, Amherst, Massachusetts 01003, United States*

Complete contact information is available at: https://pubs.acs.org/10.1021/acs.biomac.0c01767

Notes

The authors declare no competing financial interest.

■ ACKNOWLEDGMENTS

This work was supported by NIH R01 GM080532 and GM136395. F.A. was supported by the UMASS BTP Program (NIH T32 GM108556). We thank the B. Huang lab at UCSF for the HEK293 cell line stably expressing GFP1−10. We likewise thank Dr. Jim Chambers at the UMASS Light Microscopy Center and Dr. Amy Burnside at the UMASS Flow Cytometry center. We also thank Christopher Hango, Tew Lab at UMASS, for productive scientific conversations.

■ REFERENCES

(1) Gu, Z.; Biswas, A.; Zhao, M.; Tang, Y. Tailoring Nanocarriers for Intracellular Protein Delivery. *Chem. Soc. Rev.* **2011**, *40*, 3638−3655.

(2) Galliani, M.; Tremolanti, C.; Signore, G. Nanocarriers for Protein Delivery to the Cytosol: Assessing the Endosomal Escape of Poly(lactide-*co*-glycolide)-Poly(ethylene imine) Nanoparticles. *Nanomaterials* **2019**, *9*, 652.

(3) Leader, B.; Baca, Q. J.; Golan, D. E. Protein Therapeutics: A Summary and Pharmacological Classification. *Nat. Rev. Drug Discovery* **2008**, *7*, 21−39.

(4) Pisal, D. S.; Kosloski, M. P.; Balu-Iyer, S. V. Delivery Of Therapeutic Proteins. *J. Pharm. Sci.* **2010**, *99*, 2557−2575.

(5) Lv, J.; Fan, Q.; Wang, H.; Cheng, Y. Polymers for Cytosolic Protein Delivery. *Biomaterials* **2019**, *218*, 119358.

(6) Ren, L.; Lv, J.; Wang, H.; Cheng, Y. A Coordinative Dendrimer Achieves Excellent Efficiency in Cytosolic Protein and Peptide Delivery. *Angew. Chem., Int. Ed.* **2020**, *59*, 4711−4719.

(7) Zhang, Y.; Røise, J. J.; Lee, K.; Li, J.; Murthy, N. Recent Developments in Intracellular Protein Delivery. *Curr. Opin. Biotechnol.* **2018**, *52*, 25−31.

(8) Lu, Y.; Sun, W.; Gu, Z. Stimuli-Responsive Nanomaterials for Therapeutic Protein Delivery. *J. Controlled Release* **2014**, *194*, 1−19.

(9) Fu, A.; Tang, R.; Hardie, J.; Farkas, M. E.; Rotello, V. M. Promises and Pitfalls of Intracellular Delivery of Proteins. *Bioconjugate Chem.* **2014**, *25*, 1602−1608.

(10) Dutta, K.; Hu, D.; Zhao, B.; Ribbe, A. E.; Zhuang, J.; Thayumanavan, S. Templated Self-Assembly of a Covalent Polymer Network for Intracellular Protein Delivery and Traceless Release. *J. Am. Chem. Soc.* **2017**, *139*, 5676−5679.

(11) Smith, S. A.; Selby, L. I.; Johnston, A. P. R.; Such, G. K. The Endosomal Escape of Nanoparticles: Toward More Efficient Cellular Delivery. *Bioconjugate Chem.* **2019**, *30*, 263−272.

(12) Shete, H. K.; Prabhu, R. H.; Patravale, V. B. Endosomal Escape: A Bottleneck in Intracellular Delivery. *J. Nanosci. Nanotechnol.* **2014**, *14*, 460−474.

(13) Leopold, P. L. Endosomal Escape Pathways for Delivery of Biologics. *Lysosomes Biol. Dis. Ther.* **2016**, *3*, 383−407.

(14) Szeto, H. H.; Schiller, P. W.; Zhao, K.; Luo, G. Fluorescent Dyes Alter Intracellular Targeting and Function of Cell-Penetrating Tetrapeptides. *FASEB J.* **2005**, *19*, 118−120.
(15) Snipstad, S.; Hak, S.; Baghirov, H.; Sulheim, E.; Mørch, Ý.; Lélu, S.; von Haartman, E.; Bäck, M.; Nilsson, K. P. R.; Klymchenko, A. S.; et al. Labeling Nanoparticles: Dye Leakage and Altered Cellular Uptake. *Cytometry, Part A* **2017**, *91*, 760−766.
(16) Dougherty, C. A.; Vaidyanathan, S.; Orr, B. G.; Banaszak Holl, M. M. Fluorophore:Dendrimer Ratio Impacts Cellular Uptake and Intracellular Fluorescence Lifetime. *Bioconjugate Chem.* **2015**, *26*, 304−315.
(17) Zanetti-Domingues, L. C.; Tynan, C. J.; Rolfe, D. J.; Clarke, D. T.; Martin-Fernandez, M. Hydrophobic Fluorescent Probes Introduce Artifacts into Single Molecule Tracking Experiments Due to Non-Specific Binding. *PLoS One* **2013**, *8*, e74200.
(18) Jiang, Z.; Liu, H.; He, H.; Yadava, N.; Chambers, J. J.; Thayumanavan, S. Anionic Polymers Promote Mitochondrial Targeting of Delocalized Lipophilic Cations. *Bioconjugate Chem.* **2020**, *31*, 1344−1353.
(19) Li, Y.; Almassalha, L. M.; Chandler, J. E.; Zhou, X.; Stypula-Cyrus, Y. E.; Hujsak, K. A.; Roth, E. W.; Bleher, R.; Subramanian, H.; Szleifer, I.; et al. The Effects of Chemical Fixation on the Cellular Nanostructure. *Exp. Cell Res.* **2017**, *358*, 253.
(20) Hobro, A. J.; Smith, N. I. An Evaluation of Fixation Methods: Spatial and Compositional Cellular Changes Observed by Raman Imaging. *Vib. Spectrosc.* **2017**, *91*, 31−45.
(21) Stanly, T. A.; Fritzsche, M.; Banerji, S.; Garcia, E.; De La Serna, J. B.; Jackson, D. G.; Eggeling, C. Critical Importance of Appropriate Fixation Conditions for Faithful Imaging of Receptor Microclusters. *Biol. Open* **2016**, *5*, 1343−1350.
(22) Choi, D.-K.; Park, S.; Kim, J.; Bae, J.; Shin, S.-M.; Kim, D.-M.; Yoo, T. H.; Kim, Y.-S. Quantitative Assessment of Cellular Uptake and Cytosolic Access of Antibody in Living Cells by an Enhanced Split GFP Complementation Assay. *Biochem. Biophys. Res. Commun.* **2015**, *467*, 771−777.
(23) Milech, N.; Longville, B. A.; Cunningham, P. T.; Scobie, M. N.; Bogdawa, H. M.; Winslow, S.; Anastasas, M.; Connor, T.; Ong, F.; Stone, S. R.; et al. GFP-Complementation Assay to Detect Functional CPP and Protein Delivery into Living Cells. *Sci. Rep.* **2015**, *5*, 1−11.
(24) Lönn, P.; Kacsinta, A. D.; Cui, X. S.; Hamil, A. S.; Kaulich, M.; Gogoi, K.; Dowdy, S. F. Enhancing Endosomal Escape for Intracellular Delivery of Macromolecular Biologic Therapeutics. *Sci. Rep.* **2016**, *6*, 1−9.
(25) Schmidt, S.; Adjobo-Hermans, M. J. W.; Wallbrecher, R.; Verdurmen, W. P. R.; Bovée-Geurts, P. H. M.; Van Oostrum, J.; Milletti, F.; Enderle, T.; Brock, R. Detecting Cytosolic Peptide Delivery with the GFP Complementation Assay in the Low Micromolar Range. *Angew. Chem., Int. Ed.* **2015**, *54*, 15105−15108.
(26) Bale, S. S.; Kwon, S. J.; Shah, D. A.; Kane, R. S.; Dordick, J. S. A GFP Complementation System for Monitoring and Directing Nanomaterial Mediated Protein Delivery to Human Cellular Organelles. *Biotechnol. Bioeng.* **2010**, *107*, 1040−1047.
(27) Anson, F.; Kanjilal, P.; Thayumanavan, S.; Hardy, J. A. Tracking Exogenous Intracellular Casp-3 Using Split GFP. *Protein Sci.* **2021**, *30*, 366−380.
(28) Thompson, D. B.; Villasenor, R.; Dorr, B. M.; Zerial, M.; Liu, D. R. Cellular Uptake Mechanisms and Endosomal Trafficking of Supercharged Proteins. *Chem. Biol.* **2012**, *19*, 831−843.
(29) Freeman, E. C.; Weiland, L. M.; Meng, W. S. Modeling the Proton Sponge Hypothesis: Examining Proton Sponge Effectiveness for Enhancing Intracellular Gene Delivery through Multiscale. *J. Biomater. Sci., Polym. Ed.* **2013**, *24*, 398−416.
(30) Jiang, Z.; He, H.; Liu, H.; Thayumanavan, S. Cellular Uptake Evaluation of Amphiphilic Polymer Assemblies: Importance of Interplay between Pharmacological and Genetic Approaches. *Biomacromolecules* **2019**, *20*, 4407−4418.
(31) Siprashvili, Z.; Reuter, J. A.; Khavari, P. A. Intracellular Delivery of Functional Proteins via Decoration with Transporter Peptides. *Mol. Ther.* **2004**, *9*, 721−728.
(32) Zassler, B.; Blasig, I. E.; Humpel, C. Protein Delivery of Caspase-3 Induces Cell Death in Malignant C6 Glioma, Primary Astrocytes and Immortalized and Primary Brain Capillary Endothelial Cells. *J. Neuro-Oncol.* **2005**, *71*, 127−134.
(33) Hentzen, N. B.; Mogaki, R.; Otake, S.; Okuro, K.; Aida, T. Intracellular Photoactivation of Caspase-3 by Molecular Glues for Spatiotemporal Apoptosis Induction. *J. Am. Chem. Soc.* **2020**, *142*, 8080−8084.
(34) Fu, J.; Yu, C.; Li, L.; Yao, S. Q. Intracellular Delivery of Functional Proteins and Native Drugs by Cell-Penetrating Poly(Disulfide)S. *J. Am. Chem. Soc.* **2015**, *137*, 12153−12160.
(35) Tang, R.; Kim, C. S.; Solfiell, D. J.; Rana, S.; Mout, R.; Velázquez-Delgado, E. M.; Chompoosor, A.; Jeong, Y.; Yan, B.; Zhu, Z. J.; et al. Direct Delivery of Functional Proteins and Enzymes to the Cytosol Using Nanoparticle-Stabilized Nanocapsules. *ACS Nano* **2013**, *7*, 6667−6673.
(36) Kim, C. S.; Mout, R.; Zhao, Y.; Yeh, Y. C.; Tang, R.; Jeong, Y.; Duncan, B.; Hardy, J. A.; Rotello, V. M. Co-Delivery of Protein and Small Molecule Therapeutics Using Nanoparticle-Stabilized Nanocapsules. *Bioconjugate Chem.* **2015**, *26*, 950−954.
(37) Esteban-Fernández De Ávila, B.; Ramírez-Herrera, D. E.; Campuzano, S.; Angsantikul, P.; Zhang, L.; Wang, J. Nanomotor-Enabled PH-Responsive Intracellular Delivery of Caspase-3: Toward Rapid Cell Apoptosis. *ACS Nano* **2017**, *11*, 5367−5374.
(38) Ventura, J.; Eron, S. J.; González-Toro, D. C.; Raghupathi, K.; Wang, F.; Hardy, J. A.; Thayumanavan, S. Reactive Self-Assembly of Polymers and Proteins to Reversibly Silence a Killer Protein. *Biomacromolecules* **2015**, *16*, 3161−3171.
(39) Raghupathi, K.; Eron, S. J.; Anson, F.; Hardy, J. A.; Thayumanavan, S. Utilizing Inverse Emulsion Polymerization to Generate Responsive Nanogels for Cytosolic Protein Delivery. *Mol. Pharmaceutics* **2017**, *14*, 4515−4524.
(40) Riedl, S. J.; Shi, Y. Molecular Mechanisms of Caspase Regulation During Apoptosis. *Nat. Rev. Mol. Cell Biol.* **2004**, *5*, 897−907.
(41) Pop, C.; Salvesen, G. S. Human Caspases: Activation, Specificity, and Regulation. *J. Biol. Chem.* **2009**, *284*, 21777−21781.
(42) Raghupathi, K.; Thayumanavan, S. Nano-Armoring of Enzymes: Rational Design of Polymer-Wrapped Enzymes. In *Methods in Enzymology*; Academic Press, 2017; Vol *590*, pp 381−411.
(43) Ryu, J. H.; Bickerton, S.; Zhuang, J.; Thayumanavan, S. Ligand-Decorated Nanogels: Fast One-Pot Synthesis and Cellular Targeting. *Biomacromolecules* **2012**, *13*, 1515−1522.
(44) Li, L.; Raghupathi, K.; Yuan, C.; Thayumanavan, S. Surface Charge Generation in Nanogels for Activated Cellular Uptake at Tumor-Relevant PH. *Chem. Sci.* **2013**, *4*, 3654−3660.
(45) Jiwpanich, S.; Ryu, J. H.; Bickerton, S.; Thayumanavan, S. Noncovalent Encapsulation Stabilities in Supramolecular Nanoassemblies. *J. Am. Chem. Soc.* **2010**, *132*, 10683−10685.
(46) Liu, B.; Thayumanavan, S. Importance of Evaluating Dynamic Encapsulation Stability of Amphiphilic Assemblies in Serum. *Biomacromolecules* **2017**, *18*, 4163−4170.
(47) Xiong, X.-B.; Binkhathlan, Z.; Molavi, O.; Lavasanifar, A. Amphiphilic Block Co-Polymers: Preparation and Application in Nanodrug and Gene Delivery. *Acta Biomater.* **2012**, *8*, 2017−2033.
(48) Kataoka, K.; Harada, A.; Nagasaki, Y. Block Copolymer Micelles for Drug Delivery: Design. *Adv. Drug Delivery Rev.* **2001**, *47*, 113−131.
(49) Moraes, J.; Peltier, R.; Gody, G.; Blum, M.; Recalcati, S.; Klok, H. A.; Perrier, S. Influence of Block versus Random Monomer Distribution on the Cellular Uptake of Hydrophilic Copolymers. *ACS Macro Lett.* **2016**, *5*, 1416−1420.
(50) Kamiyama, D.; Sekine, S.; Barsi-Rhyne, B.; Hu, J.; Chen, B.; Gilbert, L. A.; Ishikawa, H.; Leonetti, M. D.; Marshall, W. F.; Weissman, J. S.; Huang, B. Versatile Protein Tagging in Cells with Split Fluorescent Protein. *Nat. Commun.* **2016**, *7*, 1−9.
(51) Jiang, X.; Yu, Y.; Chen, J.; Zhao, M.; Chen, H.; Song, X.; Matzuk, A. J.; Carroll, S. L.; Tan, X.; Sizovs, A.; et al. Quantitative Imaging of Glutathione in Live Cells Using a Reversible Reaction-

https://dx.doi.org/10.1021/acs.biomac.0c01767
Biomacromolecules XXXX, XXX, XXX−XXX

Based Ratiometric Fluorescent Probe. *ACS Chem. Biol.* **2015**, *10*, 864−874.
(52) Forman, H. J.; Zhang, H.; Rinna, A. Glutathione: Overview of Its Protective Roles, Measurement, and Biosynthesis. *Mol. Aspects Med.* **2009**, *30*, 1−12.
(53) Teo, S. L. Y.; Rennick, J. J.; Yuen, D.; Al-Wassiti, H.; Johnston, A. P. R.; Pouton, C. W. Unravelling Cytosolic Delivery of Endosomal Escape Peptides with a Quantitative Endosomal Escape Assay (SLEEQ). *bioRxiv 2020.08.20.258350* **2020**, na.
(54) Pelt, J.; Busatto, S.; Ferrari, M.; Thompson, E. A.; Mody, K.; Wolfram, J. Chloroquine and Nanoparticle Drug Delivery: A Promising Combination. *Pharmacol. Ther.* **2018**, *191*, 43−49.
(55) Erbacher, P.; Roche, A. C.; Monsigny, M.; Midoux, P. Putative Role of Chloroquine in Gene Transfer into a Human Hepatoma Cell Line by DNA/Lactosylated Polylysine Complexes. *Exp. Cell Res.* **1996**, *225*, 186−194.
(56) Heath, N.; Osteikoetxea, X.; de Oliveria, T. M.; Lazaro-Ibanez, E.; Shatnyeva, O.; Schindler, C.; Tigue, N.; Mayr, L. M; Dekker, N.; Overman, R.; Davies, R. Endosomal Escape Enhancing Compounds Facilitate Functional Delivery of Extracellular Vesicle Cargo. *Nanomedicine* **2019**, *14*, 2799−2814.
(57) Turner, J. J.; Ivanova, G. D.; Verbeure, B.; Williams, D.; Arzumanov, A. A.; Abes, S.; Lebleu, B.; Gait, M. J. Cell-Penetrating Peptide Conjugates of Peptide Nucleic Acids (PNA) as Inhibitors of HIV-1 Tat-Dependent Trans-Activation in Cells. *Nucleic Acids Res.* **2005**, *33*, 6837−6849.
(58) Du Rietz, H.; Hedlund, H.; Wilhelmson, S.; Nordenfelt, P.; Wittrup, A. Imaging Small Molecule-Induced Endosomal Escape of SiRNA. *Nat. Commun.* **2020**, *11*, 1−17.
(59) Cervia, L. D.; Chang, C. C.; Wang, L.; Yuan, F. Distinct Effects of Endosomal Escape and Inhibition of Endosomal Trafficking on Gene Delivery via Electrotransfection. *PLoS One* **2017**, *12*, e0171699.
(60) Dallüge, R.; Haberland, A.; Zaitsev, S.; Schneider, M.; Zastrow, H.; Sukhorukov, G.; Böttger, M. Characterization of Structure and Mechanism of Transfection-Active Peptide-DNA Complexes. *Biochim. Biophys. Acta, Gene Struct. Expression* **2002**, *1576*, 45−52.
(61) Walsh, J. G.; Cullen, S. P.; Sheridan, C.; Lüthi, A. U.; Gerner, C.; Martin, S. J. Executioner Caspase-3 and Caspase-7 Are Functionally Distinct Proteases. *Proc. Natl. Acad. Sci. U. S. A.* **2008**, *105*, 12815−12819.
(62) McComb, S.; Chan, P. K.; Guinot, A.; Hartmannsdottir, H.; Jenni, S.; Dobay, M. P.; Bourquin, J. P.; Bornhauser, B. C. Efficient Apoptosis Requires Feedback Amplification of Upstream Apoptotic Signals by Effector Caspase-3 or -7. *Sci. Adv.* **2019**, *5*, 1−12.
(63) Bus, T.; Traeger, A.; Schubert, U. S. The Great Escape: How Cationic Polyplexes Overcome the Endosomal Barrier. *J. Mater. Chem. B* **2018**, *6*, 6904−6918.
(64) El-Sayed, A.; Futaki, S.; Harashima, H. Delivery of Macromolecules Using Arginine-Rich Cell-Penetrating Peptides: Ways to Overcome Endosomal Entrapment. *AAPS J.* **2009**, *11*, 13−22.
(65) Fuchs, S. M.; Raines, R. T. Pathway for Polyarginine Entry into Mammalian Cells. *Biochemistry* **2004**, *43*, 2438−2444.
(66) Najjar, K.; Erazo-Oliveras, A.; Mosior, J. W.; Whitlock, M. J.; Rostane, I.; Cinclair, J. M.; Pellois, J. P. Unlocking Endosomal Entrapment with Supercharged Arginine-Rich Peptides. *Bioconjugate Chem.* **2017**, *28*, 2932−2941.
(67) Gonza, D. C.; Ryu, J.; Chacko, R. T.; Zhuang, J.; Thayumanavan, S. Concurrent Binding and Delivery of Proteins and Lipophilic Small Molecules Using Polymeric Nanogels. *J. Am. Chem. Soc.* **2012**, *134*, 6964−6967.
(68) Ryu, J. H.; Jiwpanich, S.; Chacko, R.; Bickerton, S.; Thayumanavan, S. Surface-Functionalizable Polymer Nanogels with Facile Hydrophobic Guest Encapsulation Capabilities. *J. Am. Chem. Soc.* **2010**, *132*, 8246−8247.
(69) Brock, D. J.; Kustigian, L.; Jiang, M.; Graham, K.; Wang, T. Y.; Erazo-Oliveras, A.; Najjar, K.; Zhang, J.; Rye, H.; Pellois, J. P. Efficient Cell Delivery Mediated by Lipid-Specific Endosomal Escape of Supercharged Branched Peptides. *Traffic* **2018**, *19*, 421−435.
(70) Cervia, L. D.; Chang, C. C.; Wang, L.; Yuan, F. Distinct Effects of Endosomal Escape and Inhibition of Endosomal Trafficking on Gene Delivery via Electrotransfection. *PLoS One* **2017**, *12*, 1−18.
(71) Creusat, G.; Rinaldi, A. S.; Weiss, E.; Elbaghdadi, R.; Remy, J. S.; Mulherkar, R.; Zuber, G. Proton Sponge Trick for PH-Sensitive Disassembly of Polyethylenimine-Based Sirna Delivery Systems. *Bioconjugate Chem.* **2010**, *21*, 994−1002.
(72) Peeler, D. J.; Sellers, D. L.; Pun, S. H. PH-Sensitive Polymers as Dynamic Mediators of Barriers to Nucleic Acid Delivery. *Bioconjugate Chem.* **2019**, *30*, 350−365.
(73) Tang, H.; Zhao, W.; Yu, J.; Li, Y.; Zhao, C. Recent Development of PH-Responsive Polymers for Cancer Nanomedicine. *Molecules* **2019**, *24*, 4.
(74) Li, W.; Nicol, F.; Szoka, F. C. GALA: A Designed Synthetic PH-Responsive Amphipathic Peptide with Applications in Drug and Gene Delivery. *Adv. Drug Delivery Rev.* **2004**, *56*, 967−985.
(75) Morris, M. C.; Chaloin, L.; Heitz, F.; Divita, G. Translocating Peptides and Proteins and Their Use for Gene Delivery. *Curr. Opin. Biotechnol.* **2000**, *11*, 461−466.
(76) Turk, M. J.; Reddy, J. A.; Chmielewski, J. A.; Low, P. S. Characterization of a Novel PH-Sensitive Peptide That Enhances Drug Release from Folate-Targeted Liposomes at Endosomal PHs. *Biochim. Biophys. Acta, Biomembr.* **2002**, *1559*, 56−68.
(77) Kwon, E. J.; Bergen, J. M.; Pun, S. H. Application of an HIV Gp41-Derived Peptide for Enhanced Intracellular Trafficking of Synthetic Gene and SiRNA Delivery Vehicles. *Bioconjugate Chem.* **2008**, *19*, 920−927.
(78) Kwon, E. J.; Liong, S.; Pun, S. H. A Truncated HGP Peptide Sequence Retains Endosomolytic Activity and Improves Gene Delivery Efficiencies. *Mol. Pharmaceutics* **2010**, *7*, 1260−1265.
(79) Ogino, C.; Ishii, J.; Nishimura, Y.; Ezawa, R.; Takeda, K.; Kondo, A. A Display of PH-Sensitive Fusogenic GALA Peptide Facilitates Endosomal Escape from a Bio-Nanocapsule via an Endocytic Uptake Pathway. *J. Nanobiotechnol.* **2014**, *12*, 11.
(80) De La Fuente-Herreruela, D.; Monnappa, A. K.; Muñoz-Úbeda, M.; Morallón-Piña, A.; Enciso, E.; Sánchez, L.; Giusti, F.; Natale, P.; López-Montero, I. Lipid-Peptide Bioconjugation through Pyridyl Disulfide Reaction Chemistry and Its Application in Cell Targeting and Drug Delivery. *J. Nanobiotechnology* **2019**, *17*, 1−14.
(81) Kuehne, J.; Murphy, R. M. Synthesis and Characterization of Membrane-Active GALA-OKT9 Conjugates. *Bioconjugate Chem.* **2001**, *12*, 742−749.
(82) Liu, B.; Ejaz, W.; Gong, S.; Kurbanov, M.; Canakci, M.; Anson, F.; Thayumanavan, S. Engineered Interactions with Mesoporous Silica Facilitate Intracellular Delivery of Proteins and Gene Editing. *Nano Lett.* **2020**, *20*, 4014−4021.

https://dx.doi.org/10.1021/acs.biomac.0c01767
Biomacromolecules XXXX, XXX, XXX−XXX